J Therm Anal Calorim (2010) 102:425–434
DOI 10.1007/s10973-010-0977-4

Phase structure of electrospun poly(trimethylene terephthalate) composite nanofibers containing carbon nanotubes

Qian Ma · Peggy Cebe

NATAS2009 Special Issue

Abstract Nanofibrous composite mats were prepared by electrospinning of poly(trimethylene terephthalate), PTT, with multi-walled carbon nanotubes (PTT/MWCNT). Trifluoroacetic acid (TFA) and methylene chloride (MC) with volume ratio of 50/50 is a good solvent for PTT and was used as the electrospining solution. Scanning electron microscopy was used to investigate the morphology of electrospun (ES) nanofibers with 0, 0.2, 1.0, or 2.0 wt% of MWCNTs. Crystal structure of the ES mats was determined from wide angle X-ray diffraction. Thermal properties were investigated using heat capacity measurements from differential scanning calorimetry (DSC) using the three-runs method for baseline correction, heat flow amplitude calibration, and sample heat capacity determination. A model comprising three phases, a mobile amorphous fraction (MAF), rigid amorphous fraction (RAF), and crystalline fraction (C), is appropriate for ES PTT/MWCNT fibers. The phase fractions, W_i (for i = RAF, MAF or C) were determined by DSC. Crystallinity decreases very slightly with the amount of MWCNT. At the same time, a large increase in RAF was observed: W_{RAF} of PTT fiber with 2% MWCNT is twice that of neat PTT fiber. The addition of MWCNTs enhanced the PTT chain alignment and increased RAF as a result. Changes of vibrational band absorbance at 1358 and 1385 cm^{-1}, corresponding to characteristic groups, were obtained with infrared spectroscopy. The increased absorbance at 1358 cm^{-1} and decreased absorbance at 1385 cm^{-1}, with the addition of MWCNTs, strongly supports the three-phase model for ES PTT/MWCNT nanocomposites.

Q. Ma · P. Cebe (✉)
Department of Physics and Astronomy, Tufts University, Medford, MA 02155, USA
e-mail: peggy.cebe@tufts.edu

Keywords Electrospinning · Poly(trimethylene terephthalate) · Multi-walled carbon nanotubes · Rigid amorphous fraction

Introduction

Poly(trimethylene terephthalate) (PTT) is a semicrystalline polymer attracting commercial interest and belonging to the homologous series of aromatic polyesters with poly(ethylene terephthalate) PET and poly(butylene terephthalate) (PBT) [1]. This family of polymers has the structural formula [2] (Scheme 1).

It is known that the physical properties of PTT ($m = 3$) are different from those of PET ($m = 2$) and PBT ($m = 4$), which are controlled by odd-numbered methylenes in the polymer chains. Fibers made from PTT have better resilience and elastic recovery compared to PET and PBT [3] and equal or better than nylon 6 and nylon 66. As a promising material for engineering plastic and textile fiber, PTT fibers may be widely used in garments requiring good resilience and substituted for nylons in carpets and other floor coverings [3].

The existence of rigid amorphous fraction (RAF) in various semicrystalline polymers has been widely recognized. The conventional two-phase model which consists of crystalline and amorphous phases does not explain the relevant physical mechanism in the highly ordered structures of most semicrystalline polymers. The third phase, the RAF, has been introduced as an intermediate component between the crystalline and amorphous phases. RAF makes its own contribution to the bulk properties of polymers, and does not participate in the glass transition process of the mobile amorphous phase, MAF [4, 5]. It has

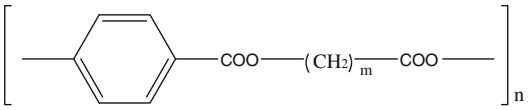

Scheme 1 Structural formula of aromatic polyesters. For PTT, $m = 3$

no contribution to the heat of fusion of the crystals either. Different mechanisms exist for the formation and relaxation behavior of RAF, depending on the polymer under study [6–9]. As for PTT, Hong et al. [10] gave a detailed report about the formation of RAF in PTT film. But until now, no systematic work has been done on the relaxation of RAF in PTT nanofibers.

Recently, Chen et al. [11] showed that the addition of MWCNTs caused polymer chains in PET electrospun fiber to become more extended, resulting in a decrease in crystallinity and an increase in RAF. Thus, electrospinning (ES) is a fiber formation technique that can be used effectively to study RAF formation and relaxation. ES has recently been widely developed as an efficient and simple technique to produce from sub-micron to nano-size fibers which may possess nanoscale surface texture, leading to different modes of interaction with other materials compared with macroscale materials [12]. A typical experimental setup of the ES process consists of syringe-like apparatus which contains polymer solution to which a high voltage is applied. When the electrical force is about to overcome the surface tension of the solution, a jet of polymer solution is ejected from the tip of the syringe needle and polymer fibers deposit onto the grounded collector [13]. For PTT, it is already known that carbon nanotubes improve the crystallization ability of the PTT matrix greatly [14]. But so far, the effects of the MWCNTs on phase structure and conformation of PTT ES fibers has not been reported.

In this article, we quantitatively establish a three-phase model for PTT electrospun fibers. The impact of multi-walled carbon nanotubes on the physical properties of PTT fibers was also investigated. Three-phase fractions and crystallization were analyzed as a function of the weight fraction of MWCNT. The multiple melting endotherms were observed and the origin of peaks was studied. Meanwhile, according to the FTIR absorbance band ratio, the chain conformation of RAF in PTT nanocomposite fibers was characterized and interpreted for the first time based on the three-phase model.

Experimental section

Materials

PTT pellets were supplied by Shell Chemical Company. MWCNTs were obtained from MER Corp. with diameter of about 140 nm, and length from 5 to 9 μm. Trifluoroacetic acid (TFA) and methylene chloride (MC) with 50/50 volume ratio were used to prepare the polymer solution at a concentration of 15 wt% for ES. MWCNTs were dispersed in hexafluoro-2-propanol (HFIP) and sonicated 24 h to minimize possible agglomerates. Then PTT pellets were dissolved in TFA/MC and sonicated overnight. All the mixture steps were carried out at room temperature. Then PTT/MWCNT solutions were prepared to obtain specific weight ratios of MWCNT to PTT: 0, 0.2, 1.0 and 2.0 wt%.

Electrospinning process

A typical experimental setup of the ES process consists of syringe-like apparatus which contains polymer solution to which a high voltage is applied. According to context, we will use the acronym, ES, to represent either the ES process, or the electrospun fiber. We used a high voltage power supply form Gamma High Voltage Research Inc., model no. ES30P-5w, to produce an applied voltage of 15 kV. The solution was loaded into a 0.55-mm inner diameter glass syringe with a copper needle electrode inside, at a working distance of 10 cm from the collector. As-spun fibers were dried in a vacuum oven for 24 h at room temperature. Samples were heated in a Mettler FP 90 hot stage for 16 h at 120 °C to effect cold crystallization.

Analytical methods

Scanning electron microscopy (SEM)

Morphology of electrospun fibers was examined using an FESEM Ultra 55 SEM at Harvard University, Center for Nanoscales Systems. Samples were fixed to the SEM holder by conducting tape, and were coated with platinum by plasma deposition.

Fourier transform infrared spectroscopy (FTIR)

A JASCO 6200 spectrometer in attenuated total reflection (ATR) mode was used to collect FTIR absorbance spectra. For each sample, 64 scans were co-added with a resolution of 4 cm^{-1} in the wave number region of 400–4000 cm^{-1}. JASCO software was used to fit the curves.

Wide angle X-ray scattering (WAXS)

Wide angle X-ray scattering was carried out using a Bruker AXS with scattering angle 2θ from 5 to 30° at wavelength = 0.1542 nm. Scattered intensity was collected for 5 min, and was corrected for air background. Two-dimensional isotropic pattern was converted to a one-dimensional pattern by integrating over a sector.

Differential scanning calorimetry (DSC)

Thermal analysis studies were carried out using a TA Instruments temperature modulated DSC (TA Q100). The instrument was calibrated with indium for the heat flow and temperature, while the heat capacity was evaluated using sapphire standard. Nitrogen gas flow of 50 ml min^{-1} was purged into the DSC cell. The sample mass was kept around 7 mg. The Al sample and reference pans are identical with an error ± 0.01 mg. The temperature modulated DSC scans (TMDSC) were performed at a heating rate of 5 °C min^{-1}, with temperature modulation amplitude of 0.796 °C and period of 60 s, using three runs to obtain the heat capacity of ES fibers. The first run is empty Al sample pan versus empty Al reference pan to obtain baseline correction. The second is sapphire standard vs. empty Al reference pan to calibrate heat flow amplitude. The third is sample vs. empty reference pan.

Results and discussion

Morphology and properties of ES fibers

SEM is used to investigate the morphology of ES fiber. The images are shown in Fig. 1a–d. According to Khilit et al.'s [14] study, an ES solution concentration of around 16% is required to prevent the appearance of beads (here, we chose 15%). It can be seen from the figures that the fibers are uniform and almost no beads exist. It has been shown in several polymers that the MWCNTs are embedded in the ES hybrid polymer nanofibers [11, 15]. Chen et al. [11] reported that most PET electrospun fibers contain naotubes while very few fibers are too thin to contain a nanotube. Prilutsky et al. [16] reported that some hybrid nanofibers exhibit at least one nanotube in the cross section using TEM. The diameter of our PTT/MWCNT composite nanofibers ranged from 400 to 900 nm which is much larger than the diameter (140 nm) of a single multi-walled carbon nanotube.

From the result of wide angle X-ray diffraction in Fig. 2, it can be seen that all as-spun fibers (exemplified by PTT/MWCNT 1%) are amorphous which is demonstrated by the absence of crystalline reflections, as shown by the bottom curve c. After cold crystallization at 120 °C for 16 h, the growth of the crystalline lamellae in samples with different amount of MWCNTs is revealed by the emergence of Bragg peaks in the WAXS profiles, as shown by curves a (2% MWCNTs) and b (0.2% MWCNTs). Comparing these two results, we observe that similar scattering patterns were obtained for the four samples (other compositions are not shown in the interest of brevity) which indicates that there is no apparent change in the crystalline structure.

Melting behavior of PTT ES fibers

The DSC results of neat PTT fibers cold-crystallized isothermally at different temperatures ranging from 180 to 212 °C are shown in Fig. 3. Each sample was cold crystallized at fixed crystallization temperature, T_C, for various times to guarantee the completion of crystallization. The heat flow has been normalized for sample mass. The curves are presented with the same scaling, but are displaced vertically for clarity. Triple or double endothermic peaks were observed depending on T_C. These endothermic peaks were labeled as Peak I, II, and III with increasing temperature. According to Srimoaon et al. [17], PTT samples

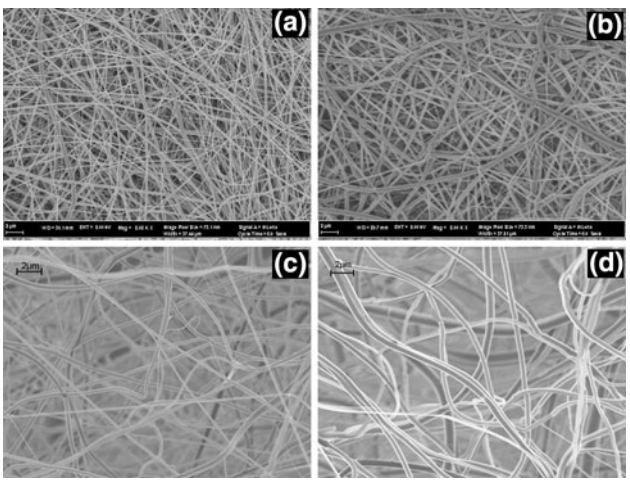

Fig. 1 SEM images of as-spun PTT/MWCNT ES nanofibers, with wt% of MWCNTs: **a** 0, **b** 0.2, **c** 1.0, and **d** 2.0. Scale bar is 2 μm. Thinner layers are shown in **b** and **d**

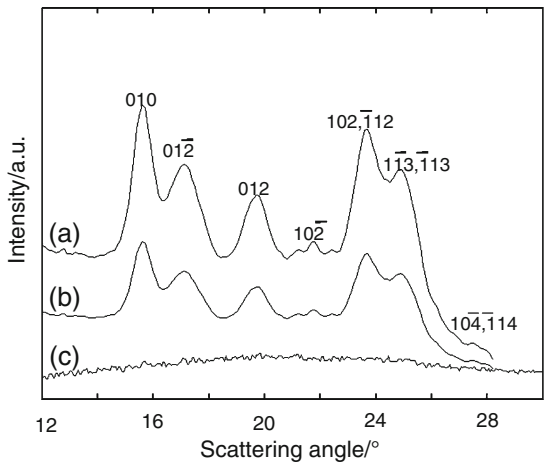

Fig. 2 WAXS diffraction patterns (intensity vs. scattering angle, 2θ, at $\lambda = 0.154$ nm) for: **a** PTT ES fibers with 2.0% MWCNT, heat-treated at 120 °C for 16 h. **b** PTT ES fiber with 0.2% MWCNT, heat-treated at 120 °C for 16 h. **c** ES PTT fibers with 1.0% MWCNT, as spun. Miller indices [15] are shown above the diffraction peaks

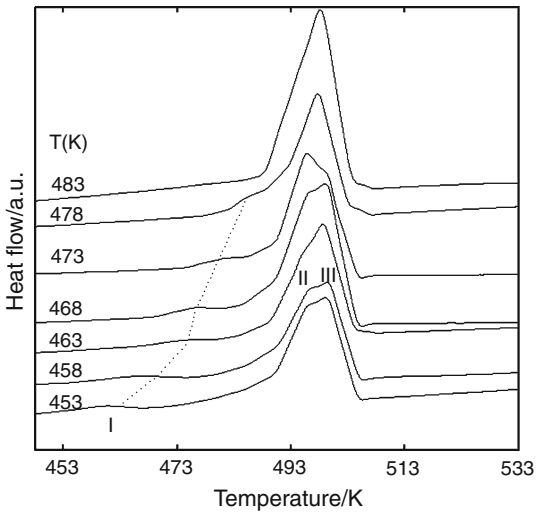

Fig. 3 DSC scans at 5 °C/min of the melting of neat ES PTT fibers isothermally cold-crystallized at different temperatures as indicated

exhibit triple peaks (for T_C lower than 192 °C (465 K)), double peaks (for T_C greater than 192 °C), or a single endothermic peak, as well as a not-apparent minor peak, usually called the "annealing peak", close to each corresponding T_C. However, in PTT fiber, the so-called minor peak is clearly observed, and with two additional peaks in the high temperature region, totally three peaks are present in PTT ES fibers, rather than the four endothermic peaks seen in PTT films [17].

Peak I is observed for all samples, and occurs always about 10–15 °C above the crystallization temperature. It shifts to high temperature and eventually merges with Peak II with increasing crystallization temperature. Peak II can be observed for samples crystallized at T_C above 175 °C (448 K) and shifts to high temperature as crystallization temperature increases. It initially develops as a shoulder, and increases in size along with a rise of temperature. Peak III exists only for samples crystallized at temperatures below 205 °C (478 K).

In order to further investigate the multi-melting phenomenon, PTT ES fibers were cold crystallized to different extents at 192 and 205 °C. The crystallization time varied from 5 to 300 min. The melting behavior is shown in Fig. 4a, b. In order to prevent further crystallization during a cooling process, the samples were heated directly from T_C to the melt. Peak I increased in size and shifted gradually to high temperature with an increase of crystallization time at both crystallization temperatures. For PTT ES fibers cold crystallized at 192 °C, Peak II increased in magnitude and shifted to higher temperature slightly as crystallization time increases. Peak III was unable to be observed in the initial time (5 min), but then it stayed constant regardless of time. Samples crystallized at 205 °C show triple melting peaks with shorter crystallization periods, while only two

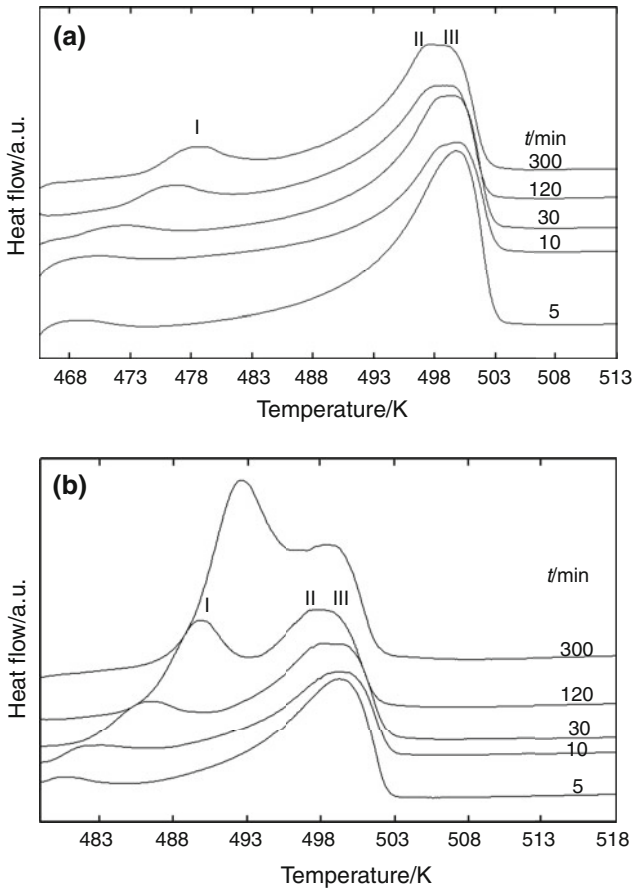

Fig. 4 DSC scans at 5 °C/min. of the melting of neat ES PTT fibers, after crystallization at different times as indicated. Crystallization temperatures are: **a** 192 °C and **b** 205 °C

peaks can be observed for samples crystallized for a relatively longer time. Peak I increased substantially with crystallization time, and eventually merged with Peak II. Peak III is not present at the initial stage, and after it appears, it remains constant in both size and position. More discussion about the attribution of melting peaks will be carried out in the following sections.

Characterization of RAF in PTT/MWCNT ES fibers

Samples were heated to 120 °C and held for 16 h in order to be fully crystallized and guarantee solvent removal. The specific reversing heat capacity of PTT/MWCNT fibers is shown in Fig. 5a–d. The degree of crystallinity of PTT/MWCNT ES fibers is determined from the endothermic area of the heat flow vs. temperature curve measured against a baseline interpolated by the procedure outlined by Hohne [18]:

$$W_C = \Delta H_{meas}/\Delta H_f \quad (1)$$

where ΔH_{meas} is the measured heat of fusion of the semicrystalline polymer while $\Delta H_f = 139.8$ J/g is the heat

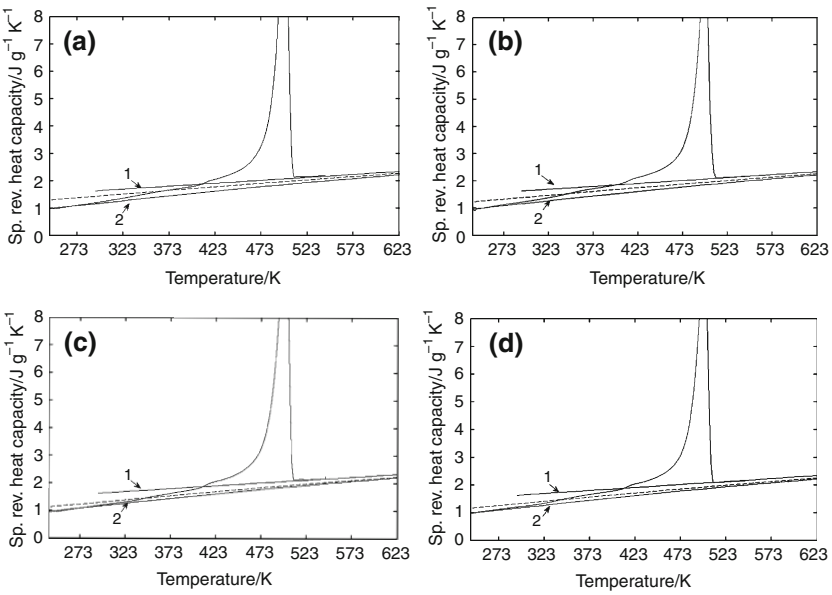

Fig. 5 Specific reversing heat capacity (*solid curve*) from TMDSC for ES PTT/MWCNT fibers at nanotube concentrations of: **a** 0%, **b** 0.2%, **c** 1.0%, and **d** 2.0%. The *dashed lines* are calculated baseline heat capacity determined form Eq. 3. C_p^{liquid} (*line 1*) and C_p^{solid} (*line 2*) are the heat capacities of 100% liquid and 100% solid from the ATHAS data bank [20]

of fusion of 100% crystalline PTT [19]. The solid lines in Fig. 5 represent the values of C_p^{solid} and C_p^{liquid}, taken from ATHAS data bank [20] and by private communication with Prof. M. Pyda. There is good agreement between the measured heat capacity and the heat capacity for homopolymer PTT below T_g as well as above the melting point. The dashed line is the calculated heat capacity C_p^{calc} under the assumption that above T_g all the mobile amorphous fraction, MAF, has relaxed to the mobile liquid state, and only the crystals and RAF remain in the solid state. That is:

$$W_S = W_C + W_{RA} = 1 - W_{MA} \tag{2}$$

Here, W_S stands for the solid fraction. Then we may write the heat capacity as:

$$\begin{aligned} C_p^{calc}(T) &= W_S C_p^{solid}(T) + W_{MA} C_p^{liquid}(T) \\ &= W_S C_p^{solid}(T) + (1 - W_S) C_p^{liquid}(T) \end{aligned} \tag{3}$$

$$C_p^{calc}(T) = (W_C + W_{RA}) C_p^{solid}(T) + (1 - W_C - W_{RA}) C_p^{liquid}(T) \tag{4}$$

According to Eq. 3, $C_p^{calc}(T)$ is a linear temperature-dependent function of W_S, and a series of lines of $C_p^{calc}(T)$ versus T could be drawn by adopting different values of W_S. Each line intersects the specific heat capacity curve at a unique point, and each of these points corresponds to a particular value of W_S. Therefore, we could chose a set of W_S and W_{MA} ($W_{MA} = 1 - W_S$) to draw a line which passes through the point just above the fulfillment of the glass transition. Based on the solid fraction and Eq. 2, we obtain the fractions for the three phases, as shown in Table 1 for PTT/MWCNT ES fibers cold crystallized at 120 °C.

Crystallinity decreases very slightly with the amount of MWCNT. It is widely known that carbon nanotubes embedded in polymer nanofibers act as nucleating agents in polypropylene (PP) [21], Nylon 6 [22], polyacrylonitrile (PAN) [16], and PET [23]. For PTT ES fibers, the degree of crystallinity does not increase with the presence of MWCNTs. It is thought that the overall increment of crystallinity is limited due to the effect of polymer chain confinement induced by MWCNT addition [24]. Although crystallinity decreases slightly, a large increase in RAF was observed: W_{RAF} of PTT fiber with 2% MWCNT is 33%, compared to 11% in the homopolymer PTT fiber.

There are a few works that provide a review of polymer–nanotube interactions [25–27]. The matrix–nanotube binding results in an interfacial region of polymer in the

Table 1 Thermal properties and FTIR absorbance of PTT/MWCNT ES nanofibers: solid, crystal, rigid amorphous, and mobile amorphous fractions, glass transition temperature, and absorbance band ratios

Wt% MWCNT	$W_S \pm 0.01$	$W_C \pm 0.01$	$W_{RAF} \pm 0.01$	$W_{MAF} \pm 0.01$	T_g/K $\pm$ 0.2	$A_{1358}/A_{1410} \pm 0.01$	$A_{1385}/A_{1410} \pm 0.01$
0	0.51	0.40	0.11	0.49	342.8	0.72	2.78
0.2	0.55	0.38	0.17	0.45	334.2	0.77	1.55
1.0	0.64	0.37	0.27	0.36	334.0	0.96	1.58
2.0	0.70	0.37	0.33	0.30	333.4	0.98	1.59

vicinity of the interface, with morphology and properties different from the bulk. The existence of MWCNT-induced interfacial interactions between nanotubes and the polymer matrix may cause a strong restriction on the polymer chains [28]. At the adsorption layer of polymer molecules around the MWCNTs, the motions of chain units may also be more restricted than similar units in the mobile phase [28]. As a result, the reduction in segmental mobility would tend to increase RAF. This has been recently shown in other systems. Schick et al. [29] reported the existence of an immobilized fraction in PMMA/SiO_2 nanocomposite induced by the interaction of SiO_2 and PMMA.

It has been shown by TEM that MWCNTs were embedded in the nanofibers as individual elements, mostly along the fiber axis, rather than being randomly oriented [16, 30]. During the ES process, strong elongation forces lead the PTT polymer which contains MWCNT to align along the direction of MWCNT by the charged fluid jet. In other words, the addition of MWCNTs improves the alignment of polymer fibers [25]. This enhanced uniform alignment, as a good way to maximize reinforcement, results in a larger confinement of the mobility of polymer chains and cause an increase in the content of RAF as a result [16].

The glass transition temperature of the MAF decreased after the addition of MWCNTs, while T_g remains almost the same for the three samples with different amount of MWCNTs. It is believed that the addition of nano-sized inorganic additive separates the long polymer chain into shorter cooperatively rearranging (CRR) segments [10]. The relatively shorter CRR segments possess higher mobility; this results in a shift of T_g toward low temperature. On the other hand, the fact that increasing the concentration of MWCNTs does not decrease T_g further indicates a tiny content of 0.2% is sufficient to change the structure of the macromolecular chains. Considering the variation tendency of crystallinity, it is extrapolated that the enhancement of chain mobility in the MAF does not suffice to increase the possibility to crystallize.

Based on the discussions above, a model for PTT/MWCNT ES fiber is proposed, as depicted in Fig. 6. The light grey part is the RAF, which exists not only as an interphase between MAF and the crystal phases, but also occurs at the surface of the MWCNTs. With the increasing concentration of MWCNT, the interactive surface area increases, inducing more immobilized fraction.

Devitrification of RAF in PTT/MWCNT ES fibers

From the total heat capacity, two endothermic peaks can be seen for PTT/MWCNT ES fiber samples heat-treated at 120 °C, as shown in Fig. 7a–d. The low temperature endotherm is the annealing peak (T_a), while the upper one

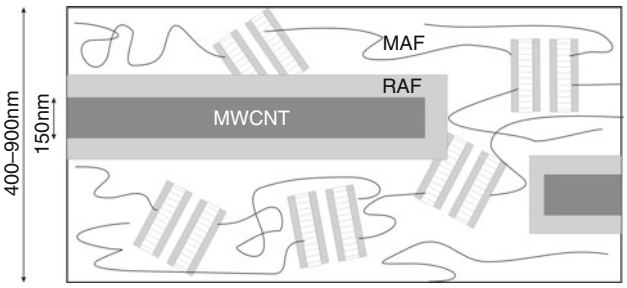

Fig. 6 Sketch of the side view of a PTT/MWCNT ES fiber. *Solid lines* represent PTT polymer chains. *Dark rectangles* represent two MWCNTs. The *grey regions* represent RAF located around the MWCNTS and the folded polymer chain crystals

is the crystal melting peak, T_m. An enthalpy relaxation peak is located around the glass transition temperature, which is caused by the discordance between the cooling rate after accomplishment of heat treatment and the DSC heating rate. When we heated the sample to above the crystallization temperature, re-annealed at 130 °C for 12 h and then cooled the sample at 5 °C/min to 30 °C, the enthalpy relaxation peak disappeared in the following re-heating in DSC.

The formation of RAF has received special interest recently. The mechanism of RAF formation is highly dependent upon the polymer studied. Usually, two possible paths have been considered to investigate the formation of RAF: RAF forms either during crystallization or during cooling after crystallization. In previous work in our group on iPS [31, 32], by means of thermal analysis, real-time X-ray scattering, and dielectric relaxation studies, RAF was shown to form in parallel to the crystalline phase. RAF was generated during isothermal crystallization due to strong constraints applied to the amorphous phase by the crystalline phase. It has also been reported that formation of RAF occurs after impingement of spherulites (at T_C), suggesting that RAF is stable at temperatures below T_C. From Fig. 7a–d, the total heat capacity and the reversing heat capacity match well just above the glass transition and before the start of the annealing peak which means that no structural change developed during this temperature range. This is similar to the conclusion that RAF is stable for temperatures below T_C [31]. There is no annealing peak observed in the reversing heat capacity curve, which indicates the association of the annealing peak with irreversible processes.

The relaxation mechanism (devitrification) of RAF depends upon the polymer under study. For polyphenylene sulfide (PPS), our group showed that RAF, created at the cold-crystallization temperature, could be relaxed upon brief heating to a temperature above the lowest crystal melting endotherm or annealing peak [31]. Liu and Petermann [33] on the basis of thermal analysis of iPS by

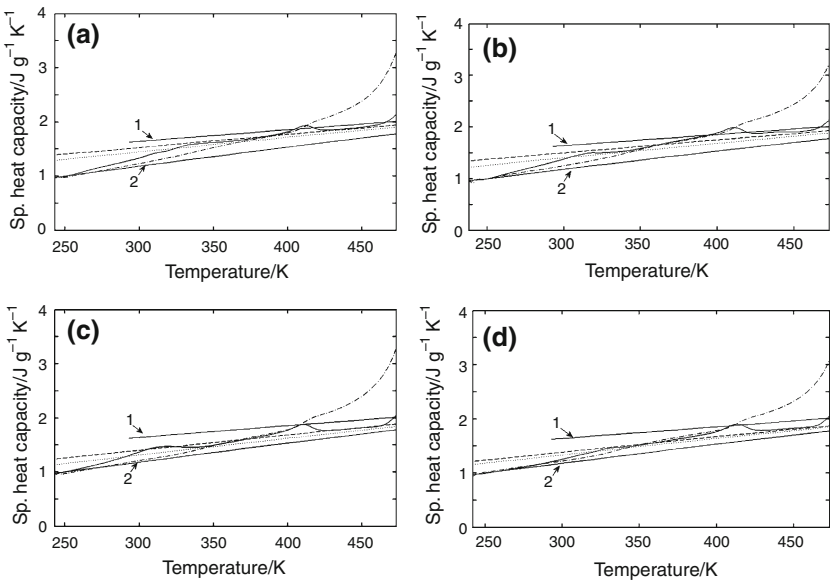

Fig. 7 Specific heat capacity vs. temperature from TMDSC, for ES PTT/MWCNT fibers at nanotube concentrations of: **a** 0%, **b** 0.2%, **c** 1.0%, and **d** 2.0%. The *solid curve* is total heat capacity; the *dash-dot curve* is reversing heat capacity. The *dotted line* is obtained from Eq. 3 based on the three-phase model; the *dashed lines* are calculated baseline heat capacity based on two-phase model. C_p^{liquid} (*line 1*) and C_p^{solid} (*line 2*) are the heat capacities of 100% liquid and 100% solid respectively, from the ATHAS data bank [20]

standard DSC, and on transmission electron microscopy studies, suggested that the annealing peak should be assigned to non-reversible relaxation process. For poly(phenylene oxide), PPO, Wunderlich et al. [34] found RAF could only be relaxed after melting the crystals. For ES fibers, Chen et al. [11] showed the relaxation of RAF does not take place until the melting of crystals in PET/MWCNT ES Fibers.

To provide evidence for relaxation of RAF in PTT/MWCNT ES fibers, total heat capacity measurements above the annealing peak for samples cold crystallized at 120 °C were studied. We predict that if the annealing peak is associated with relaxation of RAF, the system will approach to a two-phase model at a temperature just above the annealing peak, meaning that only crystals and mobile amorphous fraction will exist, and RAF devitrifies and turns into MAF during this transition. Based on this assumption, another two-phase model baseline was calculated by using Eq. 3, as shown in Fig. 7a–d. The total heat capacity matches well with the two-phase model baseline at temperatures just above the annealing peak. Using real-time WAXS (data not shown), we found there is no obvious change in the crystalline fraction before or after the annealing peak. Therefore, the change in total solid fraction is caused solely by the RAF population. We conclude that the annealing peaks in Fig. 7a–d represent the point at which the relaxation of RAF occurs, transforming RAF into equivalent amount of MAF, without obvious change in crystallinity. It is possible that crystals also are melting and recrystallizing at the location of the annealing peak, but there is no evidence of their impact on the solid fraction.

The assignment of multi-melting peaks of PTT film has been interpreted by Srimoaon's group [17]. They reported a detailed study on the multiple melting behaviors in isothermally crystallized PTT film. They concluded that the minor endoderm (annealing peak), located closed to T_C, characterized the melting of the secondary crystallites as well as their recrystallization. Based on our study of PTT fibers, Peak I is associated with the devitrification or relaxation of RAF according to heat capacity measurements, but melting and recrystallization without a change in crystallinity cannot be ruled out. As mentioned before, Peak II was observed to shift progressively to higher temperatures and increase in size with the increase of crystallization temperature, suggesting it should be attributed to the melting of crystals formed during isothermal crystallization. Peak III remains constant in magnitude and position with increasing crystallization temperature and time, which implies it might be associated with the melting of recrystallized or reorganized crystal lamellae formed during heating. For samples crystallized at 192 and 205 °C for 120 min, as the heating rate increased from 1 to 20 °C min^{-1}, Peak III decreased in area and shifted to low temperatures. This result supports a melting–recrystallization–remelting model.

This melting-reorganization process was also found in s-PP [35], iPS [36] and PET [37]. Schick et al. [37] gave clear evidence for the validity of a melting-recrystallization-remelting process for PET, using a rapid scan chip calorimeter with a heating rate as high as 2700 K S^{-1}. When the recrystallization occurs, the just-melted portion of the lamella crystallizes again and become more perfect crystal, whereas the other portion of lamella (we think this portion has higher thermal stability) goes through an annealing process.

Influence of thermal history on RAF in ES PTT/MWCNT fibers

In previous study of iPS by Xu and Cebe [31], cold crystallization of iPS results in formation of a RAF, which increases with crystallization time and temperature in a manner analogous to the development of the crystalline fraction. RAF is formed at nearly the same time as the crystalline phase, and increases more rapidly after spherulite impingement. Hong et al. [10] investigated the structural formation of PTT film at various crystallization conditions using small angle X-ray and DSC. The RAF of PTT increased with an increase of T_C. Meanwhile, there is no remarkable change in either the crystalline fraction or the lamella thickness [10]. However, for other semicrystalline polymers such as PEEK [38], lower crystallization temperature will cause less perfect crystals to form thereby causing RAF to increase. Here, the influence of crystallization temperature on RAF for PTT nanofibers was first investigated.

The fractions of each phase as a function of crystallization temperature are shown in Fig. 8a, b. For both the samples, crystallinity and RAF increase with increasing T_C, but the rate is slowing down above 140 °C. Meanwhile, MAF value shows a tendency to decline. Higher T_C would form more perfect crystal, broadening the transitional interphase thickness and inducing a larger RAF.

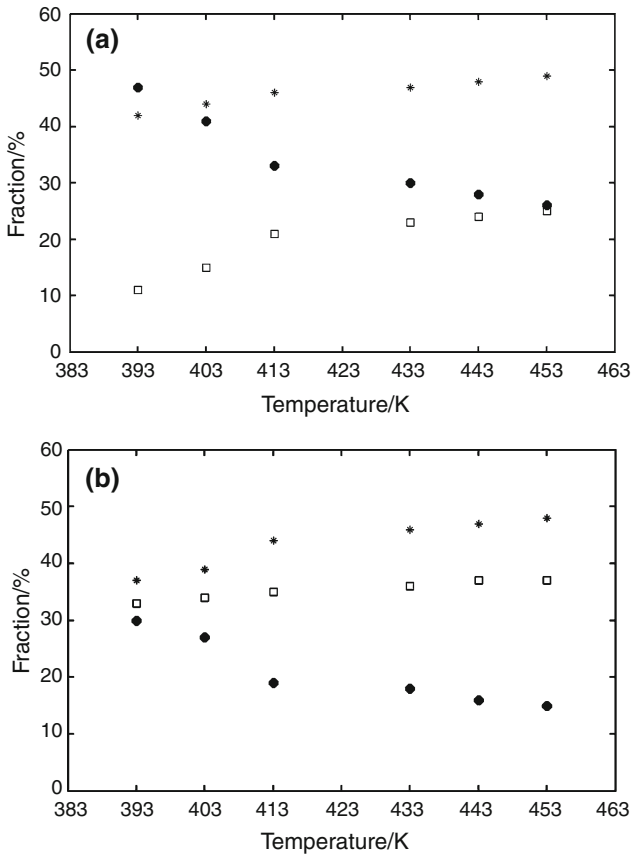

Fig. 8 Fraction of three phases versus cold-crystallization temperature for ES fibers: **a** neat PTT and **b** PTT with 2% MWCNTs. Crystal fraction (*stars*), RAF (*squares*), MAF (*circles*)

For PTT homopolymer fiber, RAF is increased by a much wider margin compared with the crystallinity, which shows only slight increase with crystallization temperature. This conforms to Hong's conclusion [10] that RAF cannot be easily incorporated into the crystalline phase. For PTT with 2% MWCNTs, the increase of RAF is inhibited, showing an increase only from 0.33 to 0.37 with crystallization temperature.

Chain conformation in ES PTT/MWCNT fibers

The conformational isomers in PTT were investigated using FTIR. Two kinds of conformational isomers exist in the PTT polymer chains, gauche (G) and trans (T). Three methylene groups between the aromatic rings provide greater flexibility to the PTT backbone compared to PET which has only two methylene groups. According to Lee and Park et al. [38], the conformation of the four bonds connected to three CH_2 units in a crystal of PTT is TGGT. The 1358 cm^{-1} band is predominantly associated with the trans conformers in the crystalline region, while 1385 cm^{-1} band is related to the gauche conformers in the amorphous regions [39]. The aromatic ring vibration band of 1410 cm^{-1} is a well-established reference band.

This set of bands assignment was questioned by Chuah [40]. He pointed out that three methylene units of PTT are arranged in a very compliant gauche–gauche conformation, which indicates that no trans conformers would exist in the crystalline regions [40]. He denoted the two CH_2 wagging vibrational bands, at 1358 cm^{-1}, to the crystalline phase gauche conformers, and at 1385 cm^{-1}, to trans conformers in the amorphous region [40].

In our study, the absorbance spectra of infrared bands were obtained (Fig. 9), and the peak areas were determined after curve fitting. The absorbance band area, A, of bands 1358 and 1385 cm^{-1} in ratio to the reference band at 1410 cm^{-1}, are listed in the last columns of Table 1. With the increase of MWCNT loading, the ratio A_{1358}/A_{1410} increases, saturating at about 1% loading. The increase indicates more and more gauche conformers were formed, in agreement with Chuah's study [40]. However, we cannot simply associate this change in gauche conformers with the crystallinity, as Chuah suggests, since the crystal fraction decreases with MWCNT addition based on our thermal analysis data. The reason for the disagreement between our results and the band assignment of Chuah [40] is that Chuah adopted a two-phase model which consists of crystalline and mobile amorphous fraction and did not take into account the RAF.

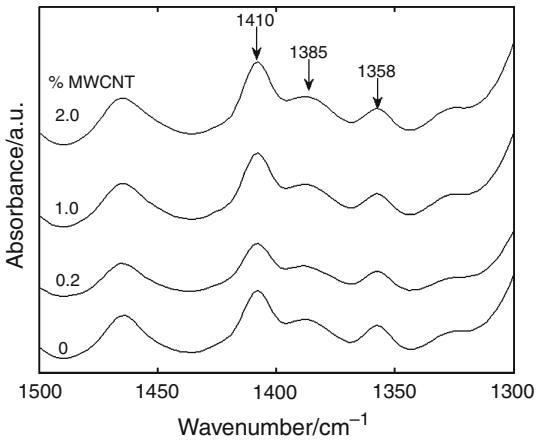

Fig. 9 FTIR absorbance spectra of ES PTT/MWCNT nanofibers with weight ratios of MWCNT as indicated

According to the results of Pyda et al. [19], in the crystalline regions, only gauche conformers exist, while in the amorphous regions, a small amount of gauche conformers is present together with a large amount of trans conformers. The increase of the ratio of A_{1358}/A_{1410} with the increase of MWCNT concentration means more and more gauche conformers were formed. However, according to the results of DSC, the crystallinity and mobile amorphous fraction both *decreased* as MWCNT concentration increased. That means the amount of gauche conformers in crystalline and mobile amorphous fraction decreased. Since the total amount of gauche shows an increasing tendency, which is manifested by the increase of A_{1358}/A_{1410}, this increasing tendency can only be realized by an increase of gauche conformers which exist within the RAF.

The A_{1385}/A_{1410} ratios for PTT/CNT ES fiber are much smaller compared to the PTT homopolymer ES fiber, and with the increase of MWCNT concentration, this ratio is nearly constant. If trans conformers were only present in MAF, the A_{1385}/A_{1410} ratio would decrease continuously as MAF decreases, instead of experiencing an initial steep fall, with first addition of MWCNT. The disproportion between the mobile amorphous fraction and trans conformer concentration shows that some amount of trans conformers must also exist within the RAF. Based on the analysis above, the addition of MWCNT inhibits the formation of trans conformers. Therefore, the trans conformer concentrations in all three PTT/CNT nanocomposites are less than that of PTT homopolymer.

The total trans conformer population is decided by a combination of two factors: the inhibition of formation of trans conformers induced by presence of MWCNT, and by the presence of RAF. It is very interesting to notice that the trans–gauche conformation of PTT/MWCNT ES fibers reported here is different from that of PET/MWCNT ES fiber [11], as shown in Table 2.

Table 2 Comparison of crystal, RAF, and MAF chain conformations for PTT and PET electrospun nanofibers

Phase	PTT	PET [11]
Crystal	Gauche	Trans
RAF	Gauche and trans	Gauche and trans
MAF	Mainly trans	Mainly gauche

Conclusions

A three-phase model is established, comprising the mobile amorphous fraction, RAF, and crystalline phase, to interpret the structure of PTT/MWCNT electrospun fibers. The addition of MWCNTs results in an obvious increase in the RAF, which indicates an enhancement in the constraints on the polymer chains in PTT composites nanofibers due to the decrease of chain mobility. Companion studies were carried out to elucidate the multiple melting peaks. From the specific heat capacity measured from DSC, it is demonstrated that the annealing peak can be associated with the devitrification of RAF, and possibly with melting and recrystallization without change of crystallinity. The lower melting peak is attributed to the melting of pre-existing crystals and the higher melting peak is the melting of recrystallized crystals.

Furthermore, for the first time, the conformation of RAF was analyzed using FTIR based on the three-phase model. This approach allows us to give a reasonable amendment to Chuah's study [40]. The disproportions between crystallinity and concentration of gauche conformers, as well as the mobile amorphous fraction and concentration of trans conformers, strongly support the existence of the third phase, RAF, in PTT/MWCNT ES nanofibers.

Acknowledgements Funding was provided by the National Science Foundation, Polymers Program of the Division of Materials Research through DMR-0602473 and thermal analysis instrumentation was obtained through the MRI Program under DMR-0520655.

References

1. Pyda M, Boller A, Grebowicz J, Chuah H, Lebedev BV, Wunderlich B. Heat capacity of poly(trimethylene terephthalate). J Polym Sci B. 1998;36:2499–511.
2. Desborough IJ, Hall IH, Neisser JZ. The structure of poly(trimethylene terephthalate). Polymer. 1979;20:545–52.
3. Kim KJ, Bae JH, Kim YH. Infrared spectroscopic analysis of poly(trimethylene terephthalate). Polymer. 2001;42:1023–33.
4. Androsch R, Wunderlich B. The link between rigid amorphous fraction and crystal perfection in cold-crystallized poly(ethylene terephthalate). Polymer. 2005;46:12556–66.
5. Chen H, Xu H, Cebe P. Thermal and structural properties of blends of isotactic with atactic polystyrene. Polymer. 2007; 48:6404–14.

6. Lu SX, Cebe P. Effects of annealing on the disappearance and creation of constrained amorphous phase. Polymer. 1996;37: 4857–63.
7. Chen HP, Cebe P. Investigation of the rigid amorphous fraction in Nylon-6. J Therm Anal Calorim. 2007;89:417–25.
8. Huo PP, Cebe P. Effects of thermal history on the rigid amorphous phase in poly(phenylene sulfide). Colloid Polym Sci. 1992;25:840–52.
9. Pak J, Pyda M, Wunderlich B. Rigid amorphous fractions and glass transitions in poly(oxy-2, 6-dimethyl-1, 4-phenylene). Macromolecules. 2003;2206:495–9.
10. Hong PD, Chuang WT, Yeh WJ, Lin TL. Effect of rigid amorphous phase on glass transition behavior of poly(trimethylene terephthalate). Polymer. 2002;43:6879–86.
11. Chen HP, Liu Z, Cebe P. Chain confinement in electrospun nanofibers of PET with carbon nanotubes. Polymer. 2009;50: 872–80.
12. Ajayan PM, Schadler LS, Braun PV. Nanocomposite science and technology. New York: Wiley-VCH; 2003.
13. Gupta P, Wilkes GL. Some investigations on the fiber formation by utilizing a side-by-side bicomponent electrospinning approach. Polymer. 2003;44:6353–9.
14. Khil MS, Kim HY, Kim MS, Park SY, Lee DR. Nanofibrous mats of poly(trimethylene terephthalate) via electrospinning. Polymer. 2004;45:295–301.
15. Kalakkunnath S, Laola DS. Dynamic mechanical and dielectric relaxation characteristics of poly(trimethylene terephthalate). Polymer. 2006;47:7085–94.
16. Prilutsky S, Zussman E, Cohen Y. The effect of embedded carbon nanotubes on the morphological evolution during the carbonization of poly(acrylonitrile) nanofibers. Nanotechnology. 2008;19: 165603.
17. Srimoaon P, Dangseeyun N, Supaphol P. Multiple melting behavior in isothermally crystallized poly(trimethylene terephthalate). Eur Polym J. 2004;40:599–608.
18. Hohne GWH. Fundamentals of differential scanning calorimetry and differential thermal analysis. In: Mathot VBF, editor. Calorimetry and thermal analysis of polymers. Munich: Hanser Publishers; 1994. p. 82–5.
19. Pyda M, Wunderlich B. Reversible and irreversible heat capacity of poly(trimethylene terephthalate) analyzed by temperature-modulated differential scanning calorimetry. J Polym Sci B. 2008;38:501–651.
20. Pyda M, editor. ATHAS data bank. http://athas.prz.edu.pl (1997).
21. Sandler J, Broza G, Nolte M, Schulte K, Lam YM, Shaffer MS. Crystallization of carbon nanotube and nanofiber polypropylene composites. J Macromol Sci B. 2003;42:479–88.
22. Jose MV, Sternert BW, Thomas V, Dean DR, Abdalla MA, Price G, Janowski GM. Morphology and mechanical properties of Nylon 6/MWNT nanofibers. Polymer. 2007;48:1096–104.
23. Ahn BW, Chi YS, Kang TJ. Preparation and characterization of multi-walled carbon nanotube/poly(ethylene terephthalate) nanoweb. J Appl Polym Sci. 2008;110:4055–63.
24. Ahn BW, Chi YS, Kang TJ. Preparation and characterization of multi-walled carbon nanotube/poly(ethylene terephthalate) nanoweb. J App Polym Sci. 2008;110:4055–63.
25. Coleman JN, Khan U, Blau WJ, Gun'ko YK. Small but strong: a review of the mechanical properties of carbon nanotube-polymer composites. Carbon. 2006;44:1624–52.
26. McCarthy B, Coleman JN, Czerw R, Dalton AB, Maiti A, et al. A microscopic and spectroscopic study of interactions between carbon nanotubes and a conjugated polymer. J Phys Chem B. 2002;106(9):2210–6.
27. Coleman JN, Ferreira MS. Geometric constraints in the growth of nanotube-templated polymer monolayers. Appl Phys Lett. 2004; 84(5):798–800.
28. Bokobza L. Multiwall carbon nanotube elastomeric composites: a review. Polymer. 2007;48:4907–20.
29. Sargsyan A, Tonoyan A, Davtyan S, Schick C. The amount of immobilized polymer in PMMA SiO_2 nanocomposites determined from calorimetric data. Eur Polym J. 2007;43:3113–27.
30. McCullen SD, Stevens DR, Roberts WA, Ojha SS, Clarke LI, Gorga RE. Morphological, electrical, and mechanical characterization of electrospun nanofiber mats containing multiwalled carbon nanotubes. Macromolecules. 2007;40:997–1003.
31. Xu H, Cebe P. Transitions from solid to liquid in isotactic polystyrene studied by thermal analysis and X-ray scattering. Polymer. 2005;46:8734–44.
32. Xu H, Cebe P. Heat capacity study of isotactic polystyrene: Dual reversible crystal melting and relaxation of rigid amorphous fraction. Macromolecules. 2004;37:2797–806.
33. Liu T, Petermann J. Multiple melting behavior in isothermally cold-crystallized isotactic polystyrene. Polymer. 2001;42: 6453–61.
34. Pak J, Pyda M, Wunderlich B. Rigid amorphous fractions and glass transitions in poly(oxy-2,6-dimethyl-1,4-phenylene). Macromolecules. 2003;36:495–9.
35. Supaphol P. Crystallization and melting behavior in syndiotactic polypropylene: origin of multiple melting phenomenon. J Appl Polym Sci. 2001;82:1083–97.
36. Minakov AA, Mordvintsev DA, Tol R, Schick C. Melting and reorganization of the crystalline fraction and relaxation of the rigid amorphous fraction of isotactic polystyrene on fast heating (30,000 K/min). ThermochimActa. 2006;42:25–30.
37. Minakov AA, Mordvintsev DA, Schick C. Melting and reorganization of poly(ethylene terephthalate) on fast heating (1000 K/s). Polymer. 2004;45:3755–63.
38. Huo PT, Cebe P. Temperature-dependent relaxation of the crystal-amorphous interphase in poly(ether ether ketone). Macromolecules. 1992;25:902–9.
39. Lee HS, Park SC, Kim YH. Structural changes of poly(trimethylene terephthalate) film upon uniaxial and biaxial drawing. Macromolecules. 2000;33:7994–8001.
40. Chuah HH. Orientation and structure development in poly(trimethylene terephthalate) tensile drawing. Macromolecules. 2001;34:6985–93.